

Routes to global glaciation: Supplementary Text

Constantin W. Arnscheidt, Daniel H. Rothman

Model formulation

In contrast to ref. [1], we consider albedo to be a smoothly varying function in temperature, reflecting the effects of partial ice coverage. Avoiding discontinuous functions in our model formulation also allows us to gain a deeper insight into the bifurcation structure of the system. The parametrization used is the following:

$$\alpha(T) = \alpha_c - (\alpha_c - \alpha_w)(0.5 + \arctan((T - T_i)/\gamma)/\pi). \quad (1)$$

Here, α_c is the limit of the albedo in a cold state, and α_w the limit of the albedo in a warm state. T_i denotes the transitional temperature at which the albedo is halfway between α_c and α_w , and γ sets the temperature scale over which this transition occurs. The sensitivity of our results to our assumptions about albedo is also further explored below. The arctan function captures the qualitative behavior of the transition, and is mathematically convenient (it is continuously differentiable). Our emphasis is on understanding the qualitative dynamics of the system; we expect that the results presented in the paper are independent of the detailed nature of the parametrization. Assuming that weathering must go to zero with decreasing T similar to the way in which $\alpha(T)$ goes towards its maximum value α_c with decreasing T , we parametrize $W(T)$ in a similar way:

$$W(T) = W_w(0.5 + \arctan((T - T_i)/\gamma)/\pi). \quad (2)$$

Here W_w represents the limit of $W(T)$ in a warm state. $W(T_0) \equiv W_0$ is another quantity of interest because the presumed stable warm climate state (T_0, P_0) requires $V = W_0$ (this can be read off the equations for the dynamical system). Since W_w and W_0 are not too far apart, we choose to set W_w according to the modern Earth weathering rate used by ref. [2], and simply let W_0 be determined by Eq. 2. The two parametrizations are plotted in Figure 1.

Our default parameters are $S_0 = 1365 \text{ W/m}^2$, $T_0 = 288 \text{ K}$ [1], $P_0 = 3 \times 10^{-4} \text{ bars}$ [1], $a = 2.2 \text{ W/m}^2/\text{K}$ [3], $b = 8 \text{ W/m}^2$ (equivalent to an assumed equilibrium climate sensitivity of 2.5 K), $\alpha_c = 0.6$, $\alpha_w = 0.2$, $\gamma = 5 \text{ K}$, $\alpha_0 = \alpha(T_0) \simeq 0.241$, $C = 2 \times 10^8 \text{ J/m}^2/\text{K}$ [1], $T_i = 273 \text{ K}$, $W_w = 70 \text{ bars/Gyr}$ [2], $W_0 = W(T_0) \simeq 62.831 \text{ bars/Gyr}$, $k = 0.1/\text{K}$ [1], $\beta = 0.5$ [4].

Model analysis

Despite the system's relative simplicity, a bifurcation analysis is challenging. Therefore, we use the numerical continuation software AUTO [5]. The result of this analysis is shown in Figure 2, with $V/W_0 = 1$. Above a stellar flux S of about 1270 W/m^2 , there exists a stable warm climate state. A fold bifurcation also gives rise to an unstable node and an unstable saddle. Below

$S = 1270 \text{ W/m}^2$, there exists a stable large-amplitude limit cycle. The existence of the limit cycle is in agreement with previous work [1, 2, 6, 7]. Finally, at even lower values of S the stable limit cycle disappears and is replaced by a stable glaciated state. Although the glaciated state does not necessarily represent complete ice cover (see below), we refer to it as a “snowball state” for simplicity.

Starting from a stable snowball state, and increasing the stellar flux, a stable limit cycle appears suddenly through a supercritical Hopf bifurcation and grows rapidly until it reaches its maximum size (Figure 3). Starting from a stable temperate state, and decreasing the stellar flux, the stable large-amplitude limit cycle appears through a saddle-node homoclinic orbit bifurcation. A second saddle-node homoclinic orbit bifurcation then generates an unstable limit cycle, which shrinks to the stable fixed point and removes its stability via a subcritical Hopf bifurcation (Figure 4). Ref. [8] describes this scenario as occurring when there is a Bogdanov-Takens bifurcation nearby in parameter space.

Figure 1 in the main text provides a map of $V - S$ parameter space and the associated stable states. The boundaries have been obtained through numerical continuation of the supercritical and subcritical Hopf bifurcations. The position of the subcritical Hopf bifurcation is a reasonable approximation to the position where the stable limit cycle disappears because the cascade of bifurcations described above (Figure 4) occurs in a very small region of parameter space.

The stable “snowball” state

In contrast to previous dynamical-system models incorporating the ice-albedo feedback and the carbonate-silicate cycle [1], our dynamical system exhibits a stable glaciated state. This state exists because $W(T)$ does not drop to zero sharply with decreasing temperature: thus, even at low temperatures any value of volcanic outgassing V can be balanced by sufficiently high P . Since the P -dependence of the weathering term in our model reflects the dependence of silicate dissolution on carbonic acid concentration [4], this state cannot represent a complete snowball: there must be an equatorial band of ocean through which CO_2 drawdown via silicate weathering can still occur. Regardless of whether this stable state is physically feasible, a real planet must eventually exhibit a single stable glaciated state as stellar flux is decreased, because the CO_2 greenhouse effect will reach its maximum before deglaciation can occur [9]. In any case, since our focus is on the boundary between the stable warm state and the stable limit cycle and on how transient glaciations may be triggered starting from the warm state, the precise nature of the glaciated state as represented in our model has no bearing on our conclusions.

Critical rate of change

We would like to know how the critical ramping rate varies as a function of time. Beyond the obvious relevance of the critical rate, understanding its scaling with time allows for the comparison of different perturbations across a vast range of timescales [10]. We obtain this scaling by perturbing the model with linearly decreasing ramps of stellar flux S over a vast range of timescales τ : the result is shown in Figure 5. All simulations are conducted with $S(t = 0) = 1300 \text{ W/m}^2$ and $V = W_0$, and S is never ramped beyond the bifurcation that occurs at $\sim 1270 \text{ W/m}^2$. We observe that the critical ramping rate decreases with time, and moreover that it scales very accurately like τ^{-1} for $\tau < 10^3$ years. This scaling can be well understood by considering the system to have

some characteristic “damping timescale”: for changes that occur faster than this timescale, what matters is not the critical rate but the critical amount [10]. At larger timescales, some of the stellar flux change is damped, and so the critical rate deviates above the τ^{-1} scaling.

Sensitivity of rate-induced glaciation to albedo assumptions

It is valuable to understand how sensitive the mechanism of rate-induced glaciation detailed in the main text is to our assumptions for the shape of $\alpha(T)$. In particular, we are interested in the effect of changing the albedo transition temperature scale γ and of changing the albedo contrast between the warm and cold limits, $\alpha_c - \alpha_w$. The latter is important in an exoplanet context because albedo values are a function of stellar spectral type: notably, Earth-like planets orbiting M-stars may have much lower ice albedo values [11, 12].

As described in the main text, rate-induced glaciation is possible whenever there is a fold (i.e. a local minimum) in the $\dot{T} = 0$ nullcline next to the warm stable state. In Figure 6, we have therefore plotted $\alpha(T)$ and $\dot{T} = 0$ curves, together with the locations of the warm stable states, for a range of γ values and for two different albedo contrasts. We see that the existence of the fold, and thus the possibility of rate-induced glaciation, appears robust to a wide range of different assumptions. Of course, increasing γ or decreasing $\alpha_c - \alpha_w$ will eventually lead to the disappearance of the fold, and rate-induced glaciation will no longer be possible. The precise boundary in $\gamma, \alpha_c - \alpha_w$ space beyond which rate-induced glaciation is no longer possible could be interesting to explore in future work, perhaps as part of a study with higher-complexity models.

Planetary heat capacity

There is an ongoing debate about the appropriate value of the planetary heat capacity C in simple models. In low-order modeling, C has generally been taken to represent the heat capacity of the ocean mixed layer [13]. Following ref. [1] we use a value of $C = 2 \times 10^8$ J/m²/K, in line with this approach. However, coupled ocean-atmosphere general circulation model simulations [14, 15] indicate that much larger fractions of the ocean must cool to freezing temperatures to allow glaciation. Therefore, we have also conducted experiments with our model with C increased by up to two orders of magnitude ($C = 2 \times 10^{10}$ J/m²/K), corresponding to the heat capacity of the entire ocean. For each value of C , we perturbed the stable warm state with a square-wave pulse of decreased stellar flux S , and studied the pulse duration necessary for rate-induced glaciation to occur. The results of the experiment are shown in Figure 7. We see that the critical instantaneous stellar flux change to initiate glaciation is only a weak function of heat capacity; however, the duration for which such a change needs to be maintained varies more strongly with heat capacity. The qualitative behavior of the model and the validity of the resulting conclusions are not affected, because the timescales of radiative equilibration and carbon cycle equilibration remain separated by multiple orders of magnitude. However, this would be an interesting topic for further investigation using more complex models.

Weathering formulation

The weathering formulation used in this paper ultimately derives from the classic work of ref. [16], which linked weathering rates to surface temperature and CO₂ levels through their effects

on silicate dissolution kinetics. This neglects the effects of seafloor weathering [17, 18]. Perhaps more importantly, recent work suggests that these dissolution kinetics only represent the dominant control on the weathering flux in a small subset of the relevant parameter space [19]; outside of this regime, various geological factors may play a more important role. While both of these considerations are important when making quantitative predictions, we argue that their omission will not affect our qualitative results.

Following Figures 2 and 3 in the main text as well as the reasoning employed above, we note that a sufficient condition for the existence of rate-induced glaciation in our model is that the $\dot{T} = 0$ nullcline is folded (i.e. has a local minimum) next to the warm stable state. Weathering terms do not enter the \dot{T} equation, only the \dot{P} equation; thus, they play no role in determining whether this fold exists. Therefore, as long as weathering provides some sort of stabilizing feedback on Earth's climate system in terms of T and/or P and operates orders of magnitude slower than radiative equilibration, the details will not affect the possibility of rate-induced glaciation.

This is illustrated in Figure 8. Here, we have plotted the $\dot{T} = 0$ nullcline, the $\dot{P} = 0$ nullcline for our default parameter settings, and the $\dot{P} = 0$ nullcline for $k, \beta = 0$ (weathering is completely independent of P and only depends on T through the effects of partial ice coverage). In all cases we retain a warm stable climate state and a fold in the $\dot{T} = 0$ nullcline; therefore, rate-induced glaciation is possible. We have also plotted a $\dot{P} = 0$ nullcline with our default parameters but with an additional constant weathering flux of $0.3 W_0$; this is to help provide intuition for the effects of seafloor weathering. Because seafloor weathering will allow the system to keep drawing down CO_2 even if T is significantly less than T_i , its inclusion will act to move the $\dot{P} = 0$ nullcline to lower P values in this regime. This will make it easier for it to intersect the cold branch of the $\dot{T} = 0$ curve, facilitating the emergence of stable glaciated states.

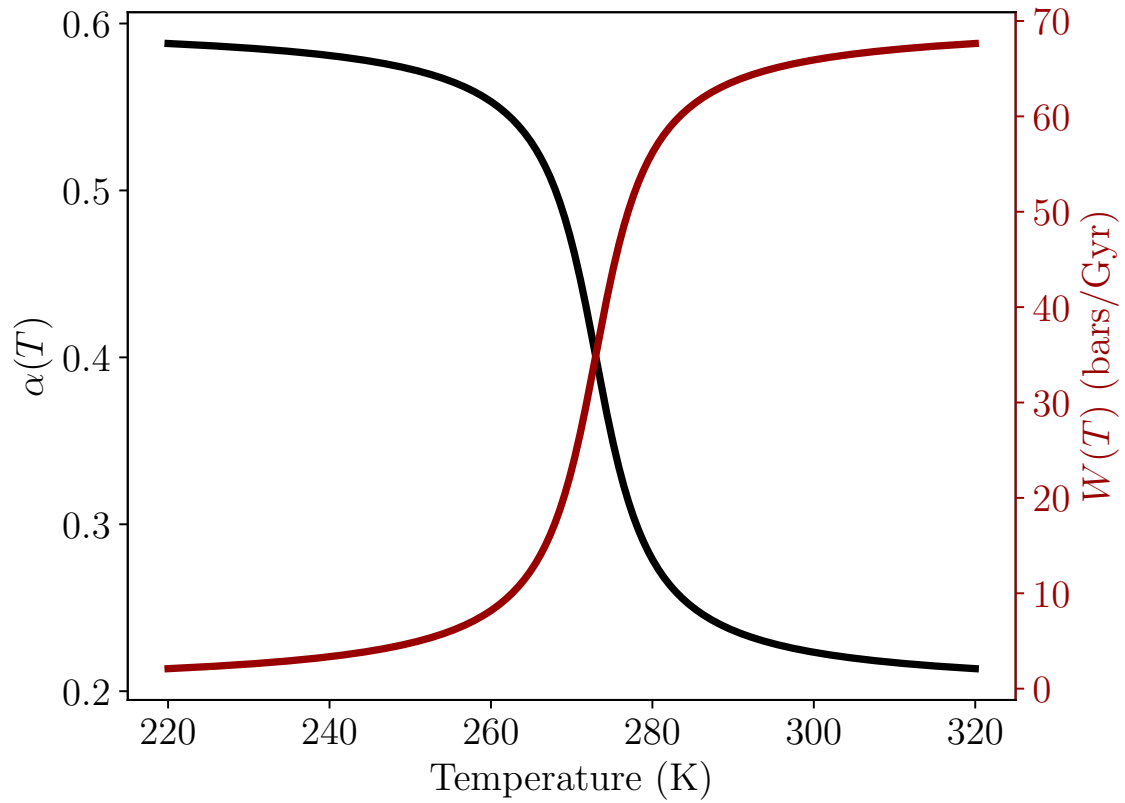


Figure 1: Parametrizations of albedo ($\alpha(T)$) and of the weathering temperature dependence due to ice coverage ($W(T)$).

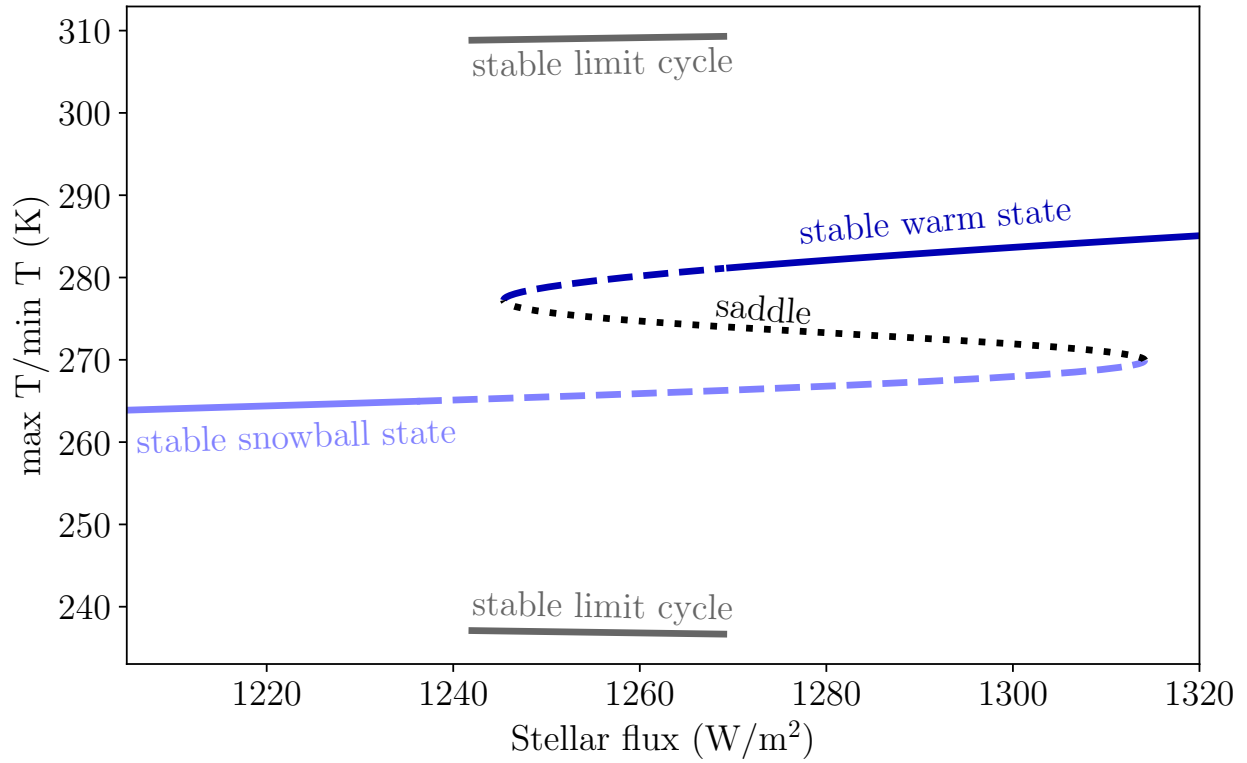


Figure 2: Bifurcation diagram with respect to stellar flux. Here, $V/W_0 = 1$. If one decreases stellar flux starting from a stable warm state, eventually a stable limit cycle will arise, in agreement with refs. [1, 2, 6, 7]

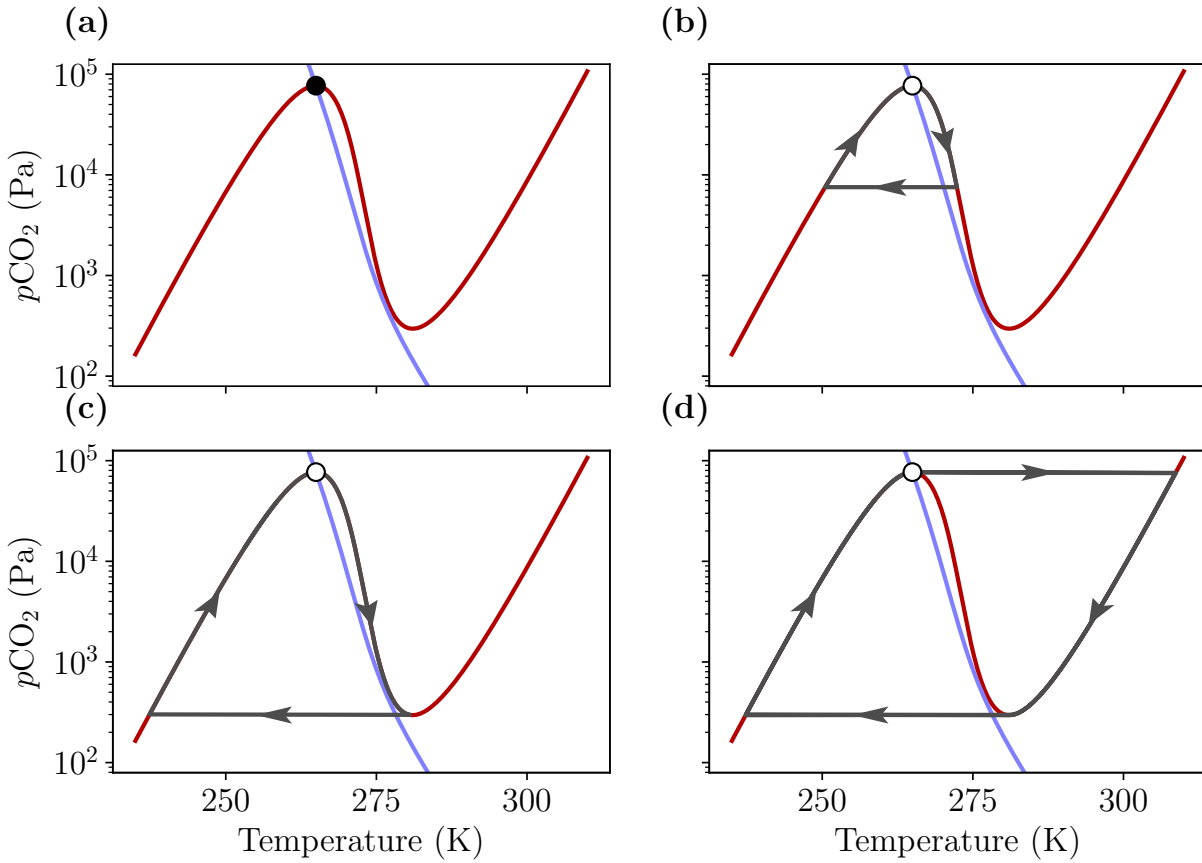


Figure 3: Appearance of the stable limit cycle from the snowball state. The blue and red curves are the \dot{P} and \dot{T} nullclines, black dots represent stable fixed points, and white dots represent unstable fixed points. As stellar flux is increased, the stable fixed point (a) undergoes a supercritical Hopf bifurcation, and a small-amplitude limit cycle appears (b). Increasing stellar flux further causes the limit cycle to expand (c), and eventually reach its maximum size (d).

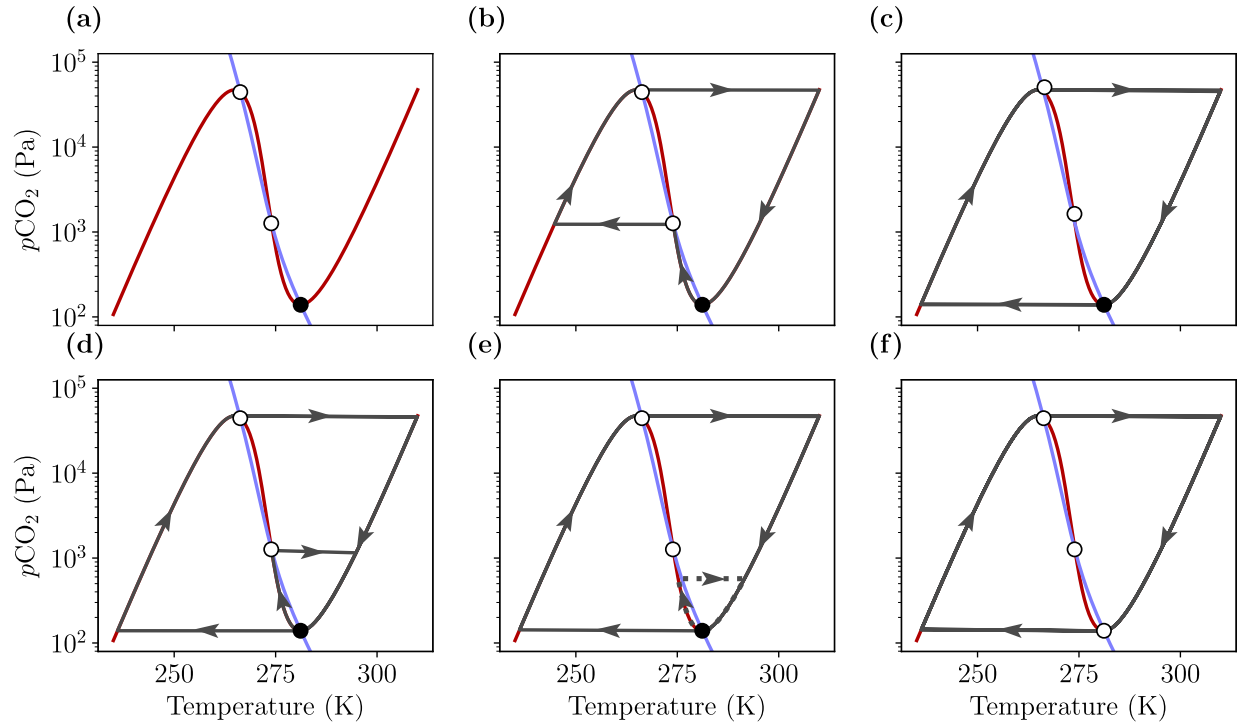


Figure 4: Appearance of the stable limit cycle from the temperate state. As before, the blue and red curves are the \dot{P} and \dot{T} nullclines, black dots represent stable fixed points, and white dots represent unstable fixed points. As stellar flux is decreased, a large homoclinic orbit forms from the saddle point (b): this rapidly grows to a limit cycle (c). As stellar flux continues to decrease, a second smaller homoclinic orbit (d) turns into an unstable limit cycle (e), which eventually shrinks to the stable fixed point and causes it to lose stability via a subcritical Hopf bifurcation (f). Only the large-amplitude limit cycle remains.

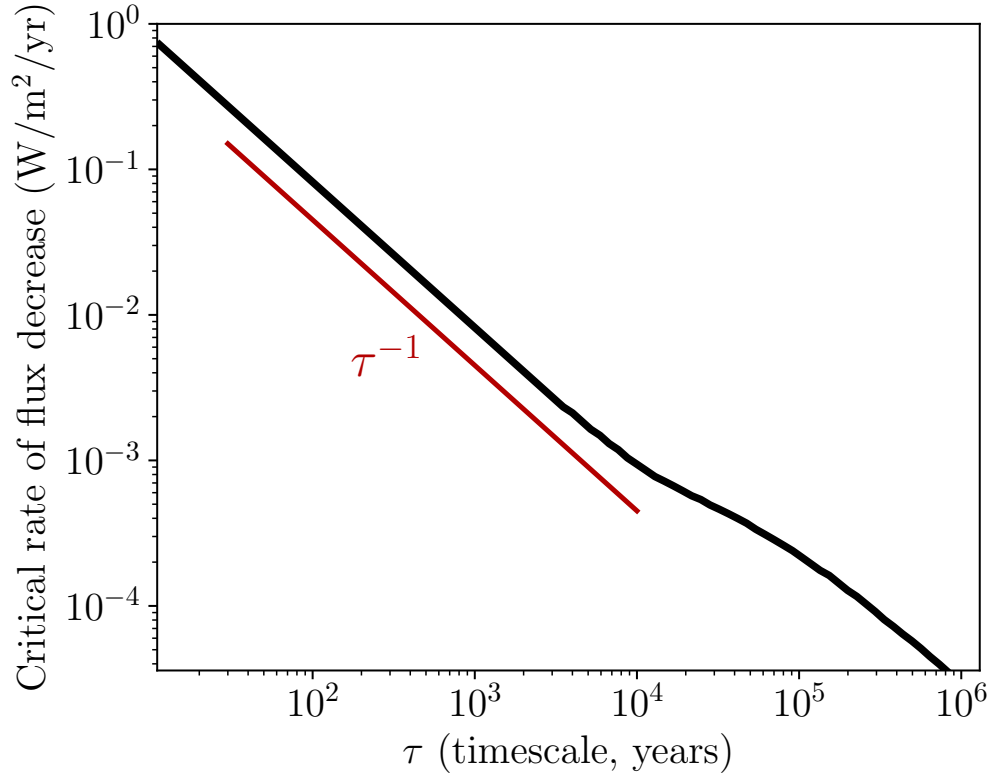


Figure 5: The critical rate of stellar flux change as a function of timescale. In all cases S is decreased linearly starting from $S = 1300 \text{ W/m}^2$, and is never ramped beyond the bifurcation that occurs at $\sim 1270 \text{ W/m}^2$. We observe that the critical ramping rate decreases with the timescale τ , and moreover that it scales very accurately like τ^{-1} for $\tau < 10^3$ years. This scaling can be well understood by considering the system to have some characteristic “damping timescale”: for changes that occur faster than this timescale, what matters is not the critical rate but the critical amount [10]. At larger timescales, some of the stellar flux change is damped, and so the critical rate deviates above the τ^{-1} scaling.

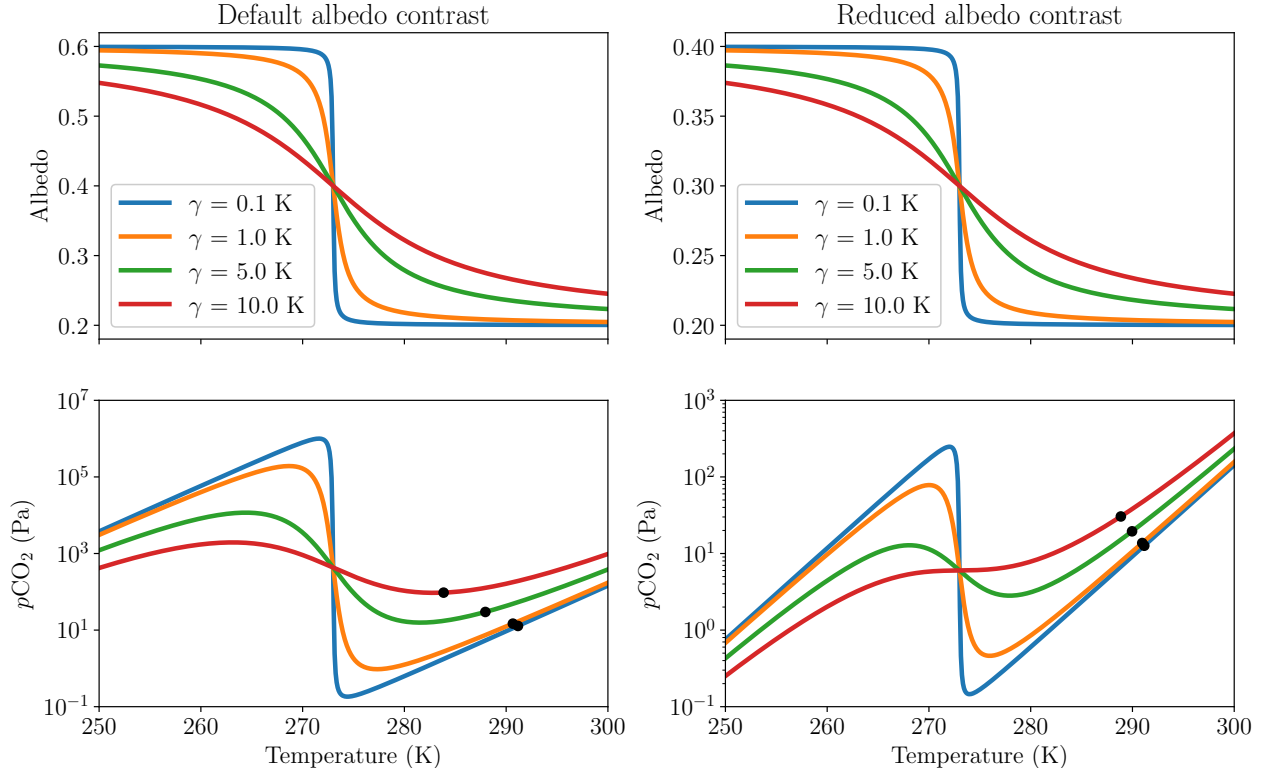


Figure 6: Exploring the sensitivity of the rate-induced glaciation mechanism to the albedo transition temperature scale γ and the albedo contrast between the warm and cold limits, $\alpha_c - \alpha_w$. $S = 1365 \text{ W/m}^2$. As described in the main text, rate-induced glaciation is possible whenever there is a fold (i.e. a local minimum) in the $\dot{T} = 0$ nullcline next to the warm stable state. We have therefore plotted $\alpha(T)$ and $\dot{T} = 0$ curves, together with the warm stable states (black dots) for a range of γ values and two different albedo contrasts. As we can see, the existence of the fold, and thus of rate-induced glaciation, appears robust to different assumptions about γ and the albedo contrast. We see that, for constant γ , decreasing the albedo contrast will eventually remove the fold, and thus the possibility of rate-induced glaciation.

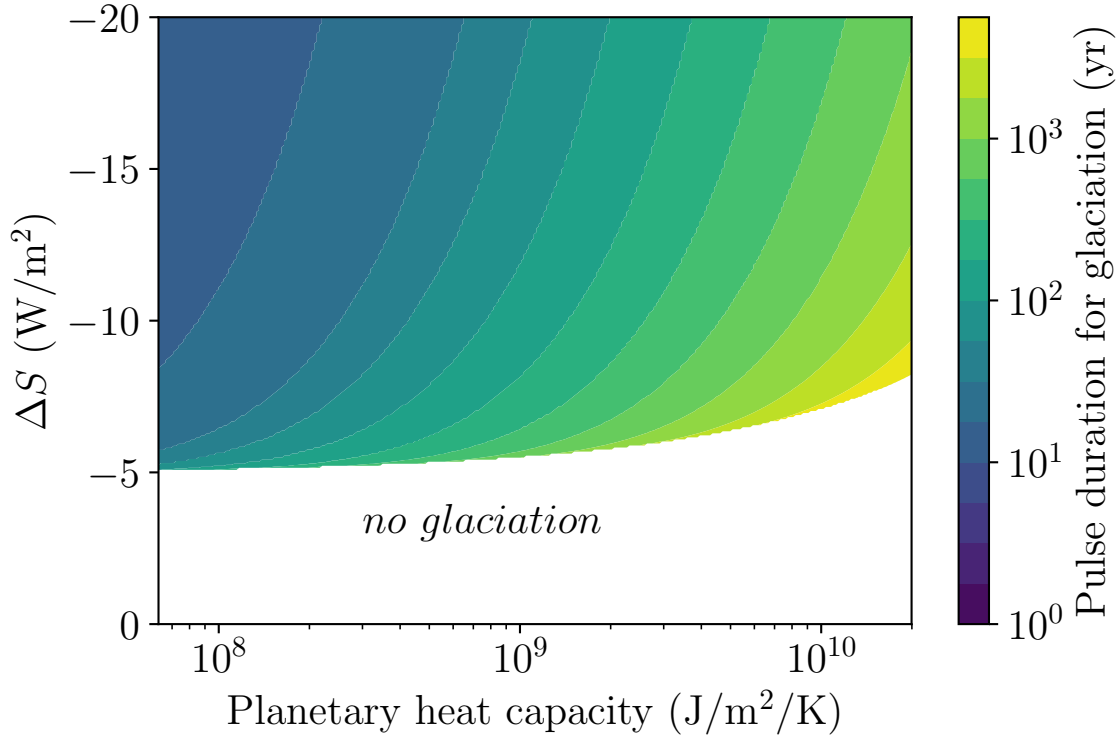


Figure 7: The duration for which an instantaneous stellar flux decrease needs to be maintained for glaciation to become inevitable. The decrease in stellar flux ΔS is implemented as a square-wave pulse. All simulations start from $S = 1300 \text{ W/m}^2$. A heat capacity of 10^8 corresponds to the mixed layer only, 10^{10} the whole ocean. We see that the critical ΔS for glaciation is largely independent of heat capacity within this range. However, at higher heat capacities the pulse needs to be maintained longer.

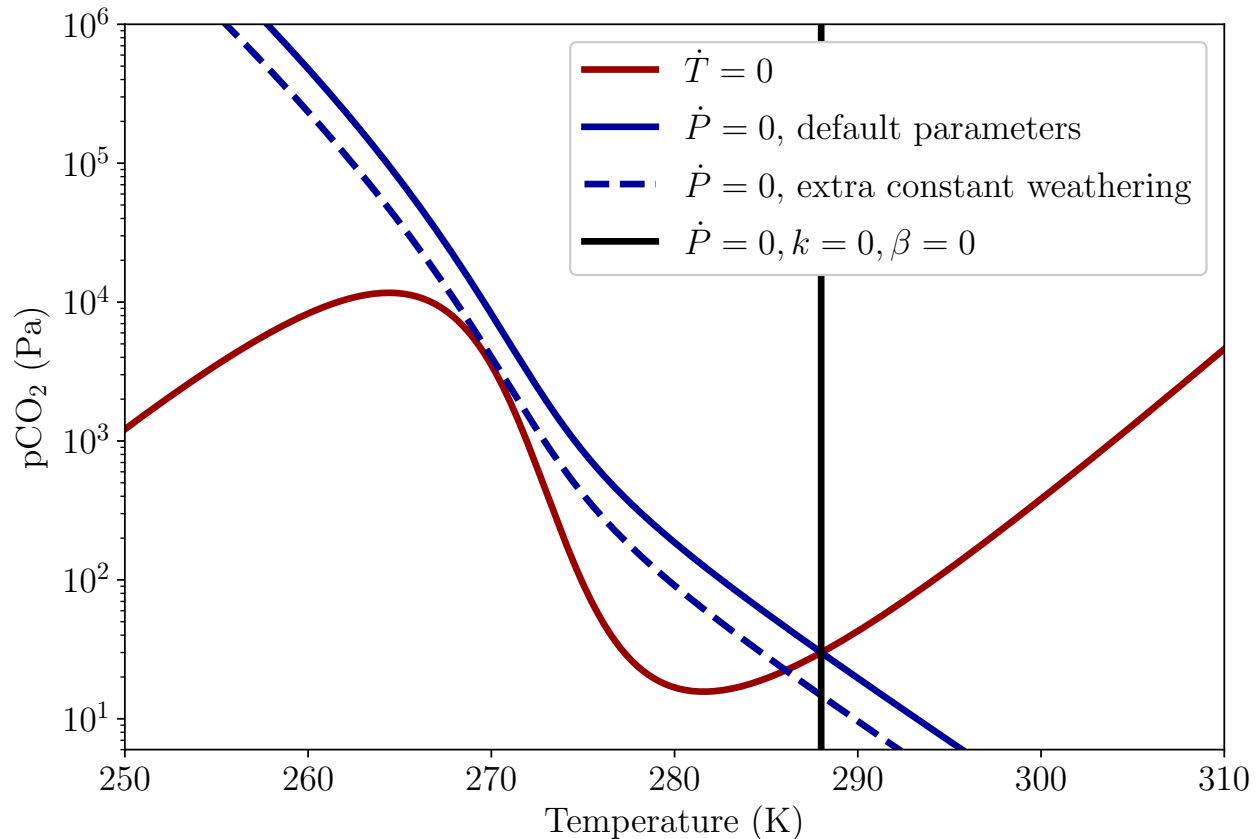


Figure 8: Exploring the effects of different weathering parametrizations on rate-induced glaciation. A sufficient condition for the existence of rate-induced glaciation in our model is that the $\dot{T} = 0$ nullcline is folded (i.e. has a local minimum) next to the warm stable state. Here, we have plotted the $\dot{T} = 0$ and $\dot{P} = 0$ curves for our default parameters, a $\dot{P} = 0$ curve where $k, \beta = 0$ (weathering is completely independent of P and only depends on T through the effects of partial ice coverage), and a $\dot{P} = 0$ curve with our default parameters but with an additional constant weathering flux of $0.3W_0$. In all cases a warm stable state exists at higher T than the location of the fold; thus, rate-induced glaciation is possible. The different formulations only affect where in parameter space the $\dot{P} = 0$ nullcline can intersect the cold branch of the $\dot{T} = 0$ nullcline, i.e. where stable glaciated climate states are possible.

References

- [1] D. S. Abbot. “Analytical investigation of the decrease in the size of the habitable zone due to a limited CO₂ outgassing rate”. *The Astrophysical Journal* 827.2 (2016), p. 117.
- [2] J. Haqq-Misra et al. “Limit cycles can reduce the width of the habitable zone”. *The Astrophysical Journal* 827.2 (2016), p. 120.
- [3] D. D. Koll and T. W. Cronin. “Earth’s outgoing longwave radiation linear due to H₂O greenhouse effect”. *Proceedings of the National Academy of Sciences* 115.41 (2018), pp. 10293–10298.
- [4] R. A. Berner. *The Phanerozoic carbon cycle: CO₂ and O₂*. Oxford University Press on Demand, 2004.
- [5] E. J. Doedel et al. *AUTO-07P: Continuation and bifurcation software for ordinary differential equations*. Tech. rep. Concordia University, 2007.
- [6] K. Menou. “Climate stability of habitable Earth-like planets”. *Earth and Planetary Science Letters* 429 (2015), pp. 20–24.
- [7] A. Paradise and K. Menou. “GCM simulations of unstable climates in the habitable zone”. *The Astrophysical Journal* 848.1 (2017), p. 33.
- [8] E. M. Izhikevich. *Dynamical Systems in Neuroscience*. MIT Press, 2007.
- [9] J. F. Kasting, D. P. Whitmire, and R. T. Reynolds. “Habitable zones around main sequence stars”. *Icarus* 101.1 (1993), pp. 108–128.
- [10] D. H. Rothman. “Characteristic disruptions of an excitable carbon cycle”. *Proceedings of the National Academy of Sciences* (2019), e1700906.
- [11] M. M. Joshi and R. M. Haberle. “Suppression of the water ice and snow albedo feedback on planets orbiting red dwarf stars and the subsequent widening of the habitable zone”. *Astrobiology* 12.1 (2012), pp. 3–8.
- [12] A. L. Shields et al. “The effect of host star spectral energy distribution and ice-albedo feedback on the climate of extrasolar planets”. *Astrobiology* 13.8 (2013), pp. 715–739.
- [13] G. North, J. Mengel, and D. Short. “Simple energy balance model resolving the seasons and the continents: Application to the astronomical theory of the ice ages”. *Journal of Geophysical Research: Oceans* 88.C11 (1983), pp. 6576–6586.
- [14] A. Voigt and J. Marotzke. “The transition from the present-day climate to a modern Snowball Earth”. *Climate dynamics* 35.5 (2010), pp. 887–905.
- [15] M. Gupta, J. Marshall, and D. Ferreira. “Triggering global climate transitions through volcanic eruptions”. *Journal of Climate* 32.12 (2019), pp. 3727–3742.
- [16] J. C. Walker, P. Hays, and J. F. Kasting. “A negative feedback mechanism for the long-term stabilization of Earth’s surface temperature”. *Journal of Geophysical Research: Oceans* 86.C10 (1981), pp. 9776–9782.
- [17] K. Caldeira. “Long-term control of atmospheric carbon dioxide; low-temperature seafloor alteration or terrestrial silicate-rock weathering?” *American Journal of Science* 295.9 (1995), pp. 1077–1114.

- [18] D. S. Abbot, N. B. Cowan, and F. J. Ciesla. “Indication of insensitivity of planetary weathering behavior and habitable zone to surface land fraction”. *The Astrophysical Journal* 756.2 (2012), p. 178.
- [19] R. J. Graham and R. Pierrehumbert. “Thermodynamic and Energetic Limits on Continental Silicate Weathering Strongly Impact the Climate and Habitability of Wet, Rocky Worlds”. *The Astrophysical Journal* 896.2 (2020), p. 115.